Power Delivery and Leakage Field Control Using an Adaptive Phased Array Wireless Power System

Benjamin H. Waters, *Student Member, IEEE*, Brody J. Mahoney, *Member, IEEE*, Vaishnavi Ranganathan, *Member, IEEE*, and Joshua R. Smith, *Member, IEEE*

***Abstract*—Efficient wireless power transfer and precise control of power delivery and leakage field strength can be achieved using a phased array wireless power transfer system. This has particular importance for charging multiple devices simultaneously, or charging devices in environments where humans or foreign objects will be in close proximity. The phased array wireless power system consists of two or more phase-synchronized power amplifiers each driving a respective transmit coil. The system can maximize power delivery to an intended receiver in one location while simultaneously minimizing power delivery and leakage fields in other locations. These functions are possible by varying the amplitude and phase of each transmitter. This paper provides an analysis of a phased array wireless power transfer system using near-field magnetically coupled resonators, and derives parameters that can be used to automatically determine the optimal magnitude and phase of each transmitter to deliver power to one or more receivers. Experimental results verify the theoretical analysis and additional features of the full system are demonstrated.**

***Index Terms*—Beamforming, magnetically coupled resonators, maximum power point tracking, phased array, wireless power transfer.**

I. Introduction

WIRELESS power transfer (WPT) using near-field magnetically coupled resonators has grown rapidly in the past decade to the point where a system comprising a single transmit (Tx) coil and single receive (Rx) coil can be found in several consumer wireless charging devices today. These systems are optimized and well-suited for applications where the mobility of the Rx coil is limited, such as wireless charging pads where the Rx coil is placed directly on top of the Tx coil. However, if the desired transmission distance is greater than the diameter of the smallest coil in the system, or if the size of the Tx coil is much larger than an Rx coil, efficiency drops drastically [1].

To avoid these design challenges, transmit coil arrays can be used to improve efficiency across a wider power transfer range. In this study, we present a phased array WPT system consisting of two or more transmit coils each driven by a power amplifier (PA) to wirelessly power one or more receivers. The transmitters are all phase-synchronized at the same frequency and the phase relationship between each transmitter can be dynamically controlled to enable constructive or destructive interference between the magnetic fields generated by each Tx coil. Not only does this system allow for increased range at which high efficiency can be achieved compared to a single transmitter system, but there are also several other advantages of this phased array WPT system.

First, maximum efficiency can be achieved anywhere within a defined volume of space, regardless of the orientation or position of the receiver by optimizing the frequency, magnitude and phase of the various transmitters. Second, maximum power regions and null-power regions can be generated simultaneously within a defined volume of space. This is desirable for systems that consist of multiple receivers because certain receivers can be targeted for charging while other receivers or even extraneous foreign objects will not be charged. Third, leakage fields can be reduced when maximum power is transferred to a targeted receiver compared to the single transmitter configuration. Minimum leakage fields are desirable for demonstrating regulatory compliance and mitigating the amount of energy induced upon foreign objects. Equation (1) as shown at the bottom of the next page.

Prior work has presented systems utilizing multiple transmit coils [2]–[5]. Johari *et al.* used multiple drive loops and Tx coils capable of improving power delivery to an Rx coil when conductive foreign objects enter the region between the coils [2]. Jadidian and Katabi present "magnetic mimo" that is capable of charging a cell-phone inside of a person's pocket nearly 40 cm away from the array of Tx coils [5]. Uchida *et al.* provide analysis for a perpendicular arrangement of two Tx coils to power mobile devices anywhere inside the Tx coil region [4]. However, these articles neglect the coupling between the Tx coils, and do not provide analysis for scaling these systems to a greater number of Tx coils. It will be shown that the coupling between the transmit coils has a significant impact on the phase at which maximum (or minimum) power is delivered to the Rx coil. Ahn and Hong present a WPT system with multiple Tx and Rx coils with intercoil coupling that uses frequency tuning to optimize the system efficiency [6]. However, frequency tuning may violate the allowable bandwidths defined by federal regulatory bodies such as the FCC [7]. This study leverages the coupling between the Tx coils and uses amplitude and phase control to overcome decreasing efficiency associated with strong coupling between Tx and Rx coils. Oodachi *et al.* show the efficiency improvement achievable with a phase-synchronized multicoil system over a single Tx coil

Manuscript received September 30, 2014; revised January 12, 2015; accepted February 10, 2015. Date of publication February 24, 2015; date of current version July 10, 2015. Recommended for publication by Associate Editor C. K. Lee.

B. H. Waters, B. J. Mahoney, and V. Ranganathan are with the Department of Electrical Engineering, University of Washington, Seattle, WA 98195 USA (e-mail: bhw2114@uw.edu; brodym@uw.edu; vnattar@uw.edu).

J. R. Smith is with the Department of Electrical Engineering and Computer Science and Engineering, University of Washington, Seattle, WA 98195 USA (e-mail: jrs@cs.washington.edu).

Color versions of one or more of the figures in this paper are available online at http://ieeexplore.ieee.org.

Digital Object Identifier 10.1109/TPEL.2015.2406673

configuration [8]. However, the study does not include circuit analysis showing the parameters required to maximize power delivery to a mobile receiver. Orientation-independent Rx coils have also been demonstrated [9]–[12]; however, the inherent efficiency limits shown for these coil designs compares unfavorably to the phased array system in this study, which also has the benefit of orientation-independence.

In this study, we present a thorough circuit analysis for a WPT system with two driven Tx coils and one Rx coil. This analysis is also generalized for a system with any number of Tx or Rx coils, and simulation results highlight some key benefits of adding more Tx coils to a phased array WPT system. The control variables for these systems are the magnitude and phase of each transmitter. We derive expressions for the magnitude and phase that maximize or minimize power delivered to the Rx coil given any coupling coefficient arrangement between the various coils. Additionally, we derive the transition point that allows the system to determine when the power delivered to the Rx coil is greater if only one transmitter is used and the other is turned off. Experimental results using our phased array WPT system are presented to verify the theoretical analysis. We demonstrate additional capabilities of the phased array WPT system including minimized leakage fields and orientation independence of the Rx coil inside of a charging box. We also show that a phased array WPT system can overcome the frequency splitting effect caused by strong coupling between Tx and Rx coils, which is prevalent in single Tx coil systems [13]. Finally, we prove that a properly configured phased array WPT system can achieve higher system-level efficiency across a larger distance range than a standard single Tx coil WPT system.

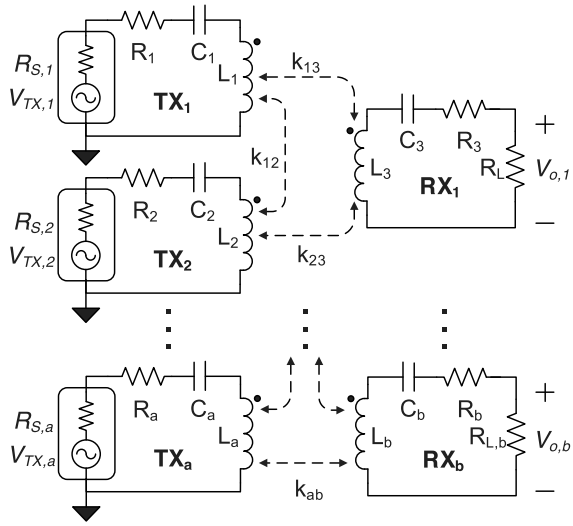

Fig. 1. Equivalent circuit diagram of a WPT system with multiple transmitters and receivers.

II. Theoretical Analysis

Beamforming using a phased array of transmit antennas has shown promise for extending the range in far-field wireless applications [14]–[16]. These systems rely on shifting the phase of one transmitter relative to the other transmitters to achieve constructive or destructive interference in the transmitted radiation pattern to maximize power delivered to a receive antenna. Mutual coupling in far-field phased array systems can significantly affect the system as spacing between antenna elements decreases [17]. Consequently, the effect of mutual coupling is typically considered parasitic and requires mitigation techniques. However, the parasitic mutual coupling can be leveraged to improve range and efficiency [18]. Near-field WPT systems must also optimize the mutual coupling between coils for efficient operation.

A. Equivalent Circuit Analysis

Fig. 1 shows the equivalent circuit model of a phased array WPT system using a Tx coils and b Rx coils. Each coil consists

$$\mathbf{V}=\begin{bmatrix} V_{\mathrm{TX},1} \\ \vdots \\ V_{\mathrm{TX},a} \\ 0 \\ \vdots \\ 0 \end{bmatrix}, \mathbf{Z}=\begin{bmatrix} Z_{\mathrm{TX},1} & j\omega M_{12} & j\omega M_{13} & j\omega M_{14} & \cdots & j\omega M_{1n} \\ \vdots & \vdots & \vdots & \vdots & \ddots & \vdots \\ j\omega M_{a1} & j\omega M_{a2} & Z_{\mathrm{TX},a} & j\omega M_{a4} & \cdots & j\omega M_{an} \\ j\omega M_{(n-b)1} & j\omega M_{(n-b)2} & j\omega M_{(n-b)3} & Z_{\mathrm{RX},1} & \cdots & j\omega M_{(n-b)n} \\ \vdots & \vdots & \vdots & \vdots & \ddots & \vdots \\ j\omega M_{n1} & j\omega M_{n2} & j\omega M_{n3} & j\omega M_{n4} & \cdots & Z_{\mathrm{RX},b} \end{bmatrix}, \mathbf{I}=\begin{bmatrix} I_{\mathrm{TX},1} \\ \vdots \\ I_{\mathrm{TX},a} \\ I_{\mathrm{RX},1} \\ \vdots \\ I_{\mathrm{RX},b} \end{bmatrix}$$

$$\mathbf{V}=\mathbf{ZI}. \tag{1}$$

$$Z_{\mathrm{TX},a}=R_{S,a}+R_{p,a}+j\omega L_a+\frac{1}{j\omega C_a}$$

$$Z_{\mathrm{RX},b}=R_{L,b}+R_{p,b}+j\omega L_b+\frac{1}{j\omega C_b}$$

$$I_i=\frac{\det(\mathbf{Z}_i)}{\det(\mathbf{Z})}: i=1,2,3\ldots n \quad V_{o,b}=I_b\times R_{L,b} \tag{2}$$

of a winding inductance $L_{a|b}$, a parasitic ac resistance $R_{a|b}$ and a series tuning capacitor $C_{a|b}$. All coils are coupled by the coupling coefficient k. Consequently, there are $n(n-2)/2$ coupling coefficients where $n = a + b$ is the total number of Tx and Rx coils in the phased array WPT system. Each Tx coil is driven at the same frequency by a phase-synchronized voltage source with adjustable magnitude and phase. Equations (3) and (4) as shown at the bottom of the page.

Using lumped-element circuit theory, the output voltage V_o at any of the receiving coils may be derived using mesh-current analysis. The matrices in (1) present the general case of n coupled coils. The $\mathbf{Z}$ matrix is square, and thus contains n^2 elements. The main diagonal comprises the reactance and resistance of each coil, which is a function of the self-inductance, tuning capacitance, source and load impedances and parasitic resistances. Using Cramer's rule, the unknown mesh currents can be determined. The $\mathbf{V}$ vector accounts for the driving voltage source of each Tx coil. The driving voltage corresponding to each Rx coil is 0 since the Rx coils are not driven.

In our proposed system, we will assume that there are a transmitters and b receivers. In each Tx coil, the resistance is the sum of the source and parasitic resistances. Similarly, in each Rx coil, the resistance is the sum of the load and parasitic resistances. Also, the load in each Rx coil is purely resistive. Thus, the output voltage of the ith coil V_{oi} is the product of load resistance and the mesh current. M_{ij} is the mutual inductance between the any two coupled inductors and can be calculated as a function of the distance and angular alignment between two coils [19]. The general solution can be found for any number of Tx and Rx coils using (1) and (2).

A phased array WPT system with more than three coils is considered in Section II-D. However, for most of this discussion, we will consider a system of three coils with two Tx coils and one Rx coil. For the three coil system, the magnitude of the voltage across R_L of the Rx coil is shown in (3).

Assuming that the frequency of the two coupled Tx coils is equivalent, phasor analysis can be used to add the contributions of each transmitter. The cumulative effort of the two Tx coils may interfere constructively or destructively, depending on the relative phase difference. In this analysis, the voltage source for the first TX coil (TX_1) is considered the reference source, with a phase $\phi_1 = 0$ and a magnitude $\alpha_1 = 1$. Thus, the phase difference $\Delta\phi = \phi_2 - \phi_1$ between the two Tx coils reduces to the phase ϕ_2 of the second transmitter's (TX_2) voltage source. Ideally, for a symmetric system with $k_{12} = 0$, if $\phi_2 = 0$ then constructive interference results in maximum V_o. Conversely, if $\phi_2 = 180°$, then the two transmitters are out of phase, which results in destructive interference and consequently a reduction in V_o. This antiphase condition minimizes power delivered to the Rx coil.

For the remainder of the three-coil discussion, α and ϕ will represent the magnitude and phase, respectively, of the transmitted signal from TX_2 such that $V_{S1} = \cos(\omega t)$ and $V_{S2} = \alpha\cos(\omega t + \phi)$. The magnitude of TX_1 will be normalized to one and the phase set to zero such that $V_{S1} = 1$ in the phasor domain. Using Euler's identity, the second source will provide the magnitude and phase offset relative to the first source such that $V_{S2} = \alpha\cos(\phi) + j\alpha\sin(\phi)$. Additionally, a symmetric system will be considered such that $L_1 = L_2 = L_3 = L$, and similarly for R and C of the coils. The same analysis can be applied to an asymmetric system, only the expressions become much larger and are not included in this paper.

B. Minimize and Maximize Power Delivered to the Receive Coil

For the objective function V_o, $\alpha_{\mathrm{opt,min}}$ represents the optimal solution that minimizes V_o. The expression for $\alpha_{\mathrm{opt,min}}$ in (4) is a function of the intercoil coupling coefficients k_{12}, k_{13} and k_{23}, the coil parameters L, R and C and ϕ. $\alpha_{\mathrm{opt,min}}$ is derived by differentiating V_o with respect to α, setting the result equal to zero, and solving for α. For a given ϕ value, $\alpha_{\mathrm{opt,min}}$ represents the magnitude that will give a relative minima of V_o at that specific phase shift. Since $\alpha_{\mathrm{opt,min}}$ is dependent on ϕ, $\alpha_{\mathrm{opt,min}}$ will only imply an absolute minimum for V_o if the phase at which V_o will be minimized ($\phi_{\mathrm{opt,min}}$) is specified.

When $k_{12} = 0$, (4) simplifies to (5). In this symmetric case, the absolute $\alpha_{\mathrm{opt,min,symm}}$ always occurs at $\phi = 180°$, which creates perfect destructive interference between the two transmitters and allows for an absolute minimum of $V_o = 0V$. If $k_{13} > k_{23}$ and $k_{12} = 0$, α_2 needs to be greater than α_1 by a factor of k_{13}/k_{23} to minimize V_o because TX_2 needs to compensate for the stronger coupling between TX_1 and the Rx coil. Alternatively, when $k_{13} < k_{23}$ and $k_{12} = 0$, α_2 needs to be less than α_1 by a factor of k_{13}/k_{23} in order to minimize V_o. In the

$$V_o = \frac{\omega R_L\left[\omega M_{12}M_{23} + jM_{13}Z_2 + (\omega M_{12}M_{13} + jM_{23}Z_1)\alpha\cos\phi + j(\omega M_{12}M_{13} + jM_{23}Z_1)\alpha\sin\phi\right]}{Z_1Z_2Z_3 + \omega^2(M_{12}{}^2Z_3 + M_{13}{}^2Z_2 + M_{23}{}^2Z_1) - 2j\omega^3M_{12}M_{13}M_{23}} \tag{3}$$

$$\alpha_{\mathrm{opt,min}} = \frac{\omega^3k_{12}LRC^2\left(k_{23}^2 - k_{13}^2\right)\sin\phi - k_{13}k_{23}\left(\omega^2R^2C^2 + k_{12}^2\right)\cos\phi}{\omega^2k_{23}^2R^2C^2 + k_{12}^2k_{13}^2} \tag{4}$$

$$\alpha_{\mathrm{opt,min,symm}} = \frac{k_{13}}{k_{23}}\cos\phi \tag{5}$$

$$\phi_{\mathrm{opt,min}} = \tan^{-1}\left[\frac{\omega^3k_{12}(k_{13}^2 - k_{23}^2)LRC^2}{k_{13}k_{23}(\omega^2R^2C^2 + k_{12}^2)}\right] \tag{6}$$

$$\phi_{\mathrm{opt,max}} = 180° - \phi_{\mathrm{opt,min}}. \tag{7}$$

case where $k_{13} \gg k_{23}$, an absolute minimum of $V_o = 0$ V is not possible to achieve unless α_2 is very large in magnitude (i.e., TX_2 outputs significantly more power than TX_1).

$\phi_{\text{opt,min}}$ is derived by differentiating V_o with respect to ϕ, setting the result equal to zero, and solving for ϕ as in (6), shown at the bottom of the previous page. Since $\phi_{\text{opt,min}}$ is independent of α, $\phi_{\text{opt,min}}$ can be calculated first, and then used to find the $\alpha_{\text{opt,min}}$ at which an absolute minimum of V_o can be achieved.

The value of α that maximizes V_o ($\alpha_{\text{opt,max}}$) always corresponds to the largest allowable value of α. This is logical because α represents the magnitude of the transmitted power: Sending more power results in a larger V_o. In a real system, $\alpha_{\text{opt,max}}$ is limited by the maximum output power capability of the PA in the WPT system. When $k_{12} = 0$, the $\alpha_{\text{opt,min}}$ simplifies to the result shown in (5), shown at the bottom of the previous page.

The value of ϕ that maximizes V_o ($\phi_{\text{opt,max}}$) always corresponds to a 180° phase shift from $\phi_{\text{opt,min}}$ as in (7), shown at the bottom of the previous page. Therefore, all four expressions for $\alpha_{\text{opt,min}}$, $\alpha_{\text{opt,max}}$, $\phi_{\text{opt,min}}$, and $\phi_{\text{opt,max}}$ can be computed directly, which implies that power can be minimized or maximized for a receiver in any known position relative to the two transmit coils.

C. Single Tx Coil Compared to Two Phase-Synchronized Tx Coils

To identify the scenarios where using two Tx coils has a higher V_o than one Tx coil, the configuration with only one active Tx coil will be compared to the case with two phase-synchronized Tx coils.

First, consider the case where the secondary transmitter is off (i.e., $\alpha = 0$). The system behaves like a standard WPT system with one Tx coil, where varying ϕ does not have any effect on V_o. We define the transition voltage ($V_{o,\text{trans}}$) as the output voltage for which the two-Tx coil system becomes greater than V_o for the single Tx coil configuration. Therefore, if $V_o > V_{o,\text{trans}}$ for a particular configuration of coupling coefficients between the three coils, then the phased array system outperforms the standard single coil system. Alternatively, if $V_o < V_{o,\text{trans}}$, then a single coil system would perform better than the phased array system and the transmitter providing less power to the load should be disabled. $V_{o,\text{trans}}$ is maximized when $k_{12} = 0$, and as k_{12} increases TX_2 begins absorbing some power from TX_1, which in turn reduces $V_{o,\text{trans}}$ in some cases.

Fig. 2 shows the simulated results for a symmetric system where $k_{12} = 0$ and $\alpha = 1$. The hashed areas represent the coupling regions in which V_o for a single Tx coil is greater than V_o for a phased array Tx configuration. In this symmetric configuration, if either $k_{23} \gg k_{13}$ or $k_{13} \gg k_{23}$, then a single Tx coil configuration will result in a higher V_o than the phased array configuration. For these regions, a two Tx coil configuration can still be used; however, the Tx coil that has lower coupling to the Rx coil should be disabled.

For a different perspective, Fig. 3 shows V_o as a function of α and ϕ. For these plots, $\alpha_2 = \alpha$ and $\alpha_1 = 1$. The magnitude of V_o is represented by the intensity of the color map. Each plot

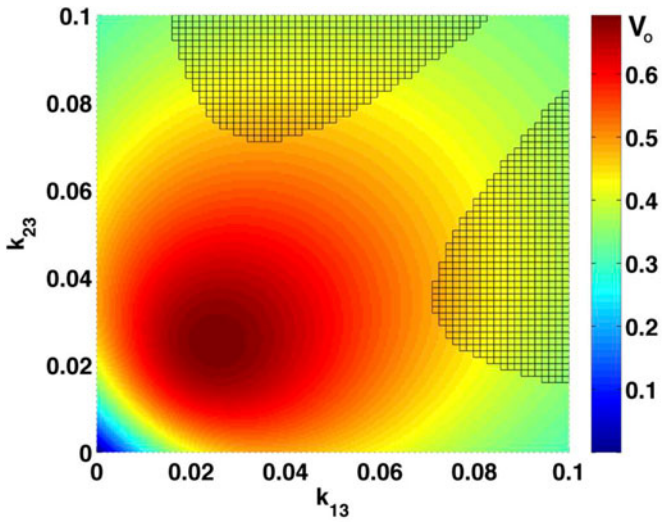

Fig. 2. V_o for a phased array WPT system with $k_{12} = 0$ and $\alpha = 1$. Hashed areas represent regions where a single Tx coil achieves greater V_o than two Tx coils.

in the panel corresponds to a different configuration of coupling coefficients k_{12}, k_{13} and k_{23}. As in Fig. 2, the dark hashed regions correspond to the scenario when a single Tx coil achieves a higher V_o than the phased array. The first row shows that for a symmetric configuration when $k_{13} = k_{23}$, the maximum V_o always occurs at $\alpha = 5$ and $\phi = 0$ while the minimum V_o always occurs at $\alpha = 1$ and $\phi = \pm 180^\circ$. The second and third rows show that when $k_{13} \neq k_{23}$, the α and ϕ values at which the maximum and minimum V_o occurs are dependent on all three coupling coefficients. As k_{12} increases, the maximum achievable V_o decreases when $k_{23} > k_{13}$. However when $k_{23} < k_{13}$, higher k_{12} improves V_o because k_{13} is overcoupled, and as more energy couples from TX_1 to TX_2, the overall energy delivered to the Rx coil at a single operating frequency increases. Corresponding to the observation made in Section II-A, to minimize V_o when k_{23} is four times greater than k_{13} and $k_{12} = 0$, α_2 must be four times less than α_1 (see Fig. 3). Similarly, to minimize V_o when k_{13} is four times greater than k_{23}, α_2 must be four times larger than α_1 (see Fig. 3).

The α value below which $V_o < V_{o,\text{trans}}$ for a given phase difference between transmitters is defined as α_{trans} (8). This parameter can be used to identify the best configuration to use (single Tx coil or phase-synchronized Tx coils) for a given configuration of coil coupling coefficients. α_{trans} is derived by solving for the value of α in (3) when it is equated to the case when TX_2 is off (i.e., $V_o|_{\alpha=\alpha_{\text{trans}}} = V_o|_{\alpha=0}$). Interestingly, α_{trans} simplifies to twice the value of $\alpha_{\text{opt,min}}$. Since α is indicative of the voltage of the transmitter, this relation implies that if a phased array system is operating at $\alpha_{\text{opt,min}}$ and $\phi_{\text{opt,min}}$, then without changing ϕ the second transmitter must output four times more power to achieve greater power delivered to the load than a single Tx coil configuration. However, this scenario would rarely be encountered in practice because the system should also tune to $\phi_{\text{opt,max}}$ to improve power delivered to the Rx coil

$$\alpha_{\text{trans}} = 2\alpha_{\text{opt,min}}. \tag{8}$$

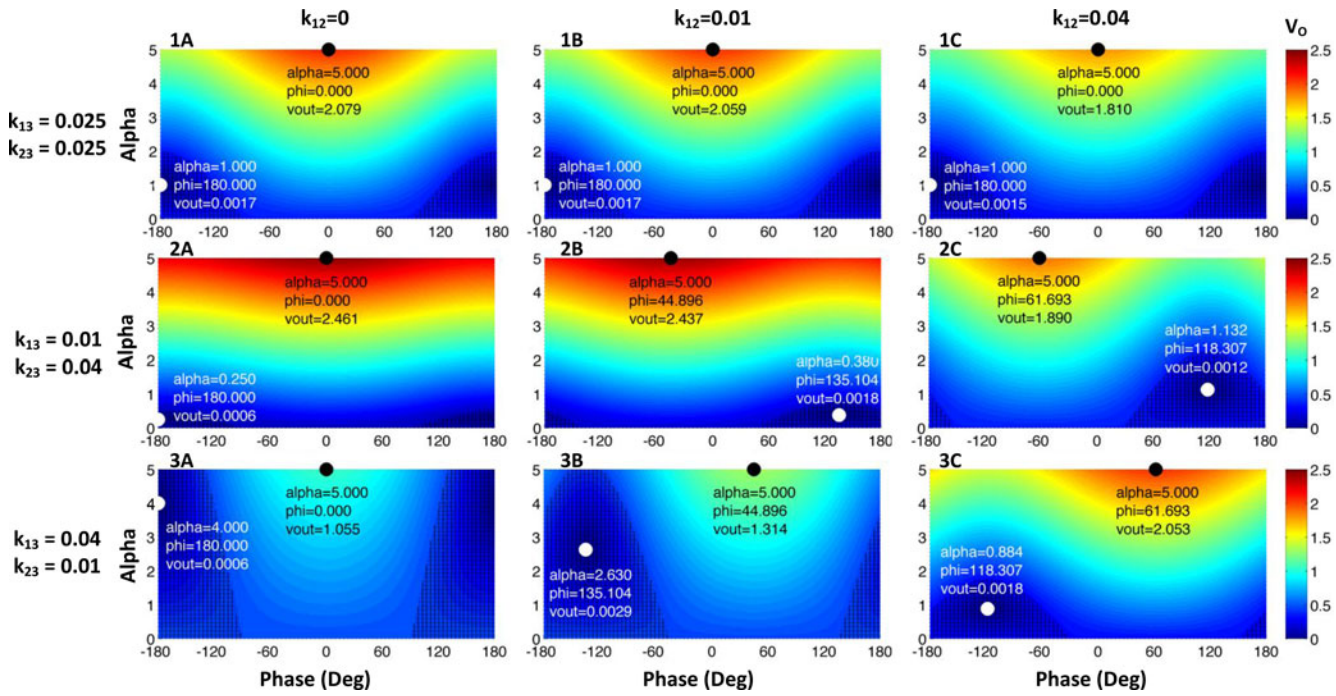

Fig. 3. V_o for a range of k_{12}, k_{13}, k_{23}, α and ϕ for a three-coil phased array system.

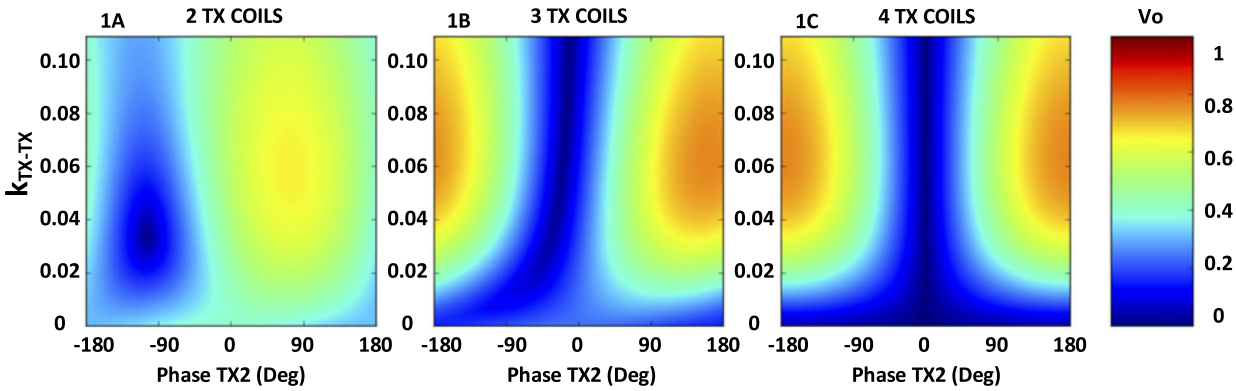

Fig. 4. V_o of one Rx coil powered by (A) two, (B) three and (C) four Tx coils.

If the goal is to minimize V_o, it is always more suitable to have two Tx coils assuming the proper $\alpha_{\text{opt,min}}$ and $\phi_{\text{opt,min}}$ are applied for the given coupling coefficients. However, if the goal is to maximize V_o it may be better to have just one Tx coil if α_{trans} is greater than the maximum allowable α that can be realized by the PA.

D. Arbitrary TX and RX Coils

As the phased array system scales with additional Tx and Rx coils, the theoretical model quickly increases in complexity. However, the added complexity introduces more degrees of freedom, which may be utilized to increase tunability of the system. For example, introducing a third Tx coil to the aforementioned two-Tx coil system provides α_3 and ϕ_3 for additional tuning knobs.

In Fig. 3, particular coupling arrangements limit the dynamic range and flexibility of the system. Fig. 4 demonstrates the benefits of adding more Tx coils to the system. The vertical axes in these plots represent $k_{\text{TX-TX}}$, which implies that all coupling coefficients between Tx coils are identical for simplicity. In practice, this can be achieved by placing the Tx coils in a geometrically symmetrical configuration. The horizontal axes represent the phase of the second Tx coil ϕ_2. From Fig. 4(A), for $k_{\text{TX-TX}} = 0.03$, a two TX coil system can achieve a minimum voltage level of nearly 0 V and a maximum voltage of 0.6 V by adjusting the phase difference between the two transmitters. However, for other values of $k_{\text{TX-TX}}$, the range of achievable output voltages is limited with only two Tx coils. With three Tx coils in Fig. 4(B), a wide range of output voltages can be achieved for nearly all values of $k_{\text{TX-TX}}$ by utilizing the additional tuning parameters ϕ_3 and α_3. For a fair comparison to the two Tx coil plot, all parameters were retained from Fig. 4(A) while $\phi_3 = 180^\circ$ and $\alpha_3 = 1$. In Fig. 4(C), a fourth Tx coil was added with $\phi_4 = -180^\circ$ and $\alpha_4 = 1$. This plot shows that the system can achieve a nulling effect with $V_o = 0$ for the entire

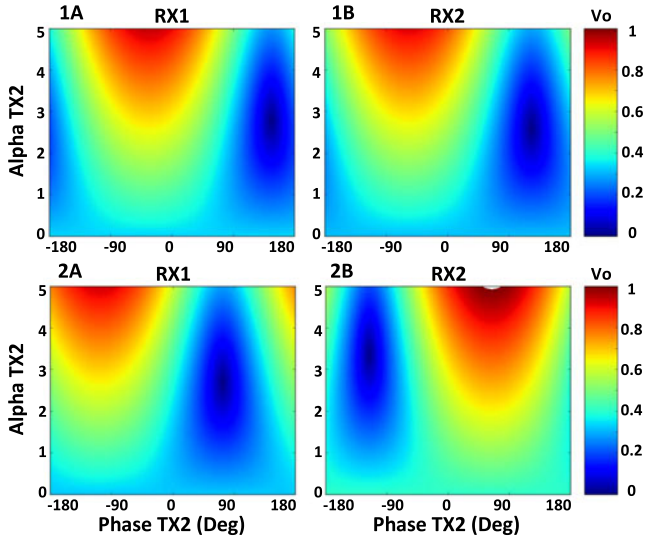

Fig. 5. V_o of two Rx coils powered simultaneously by three Tx coils.

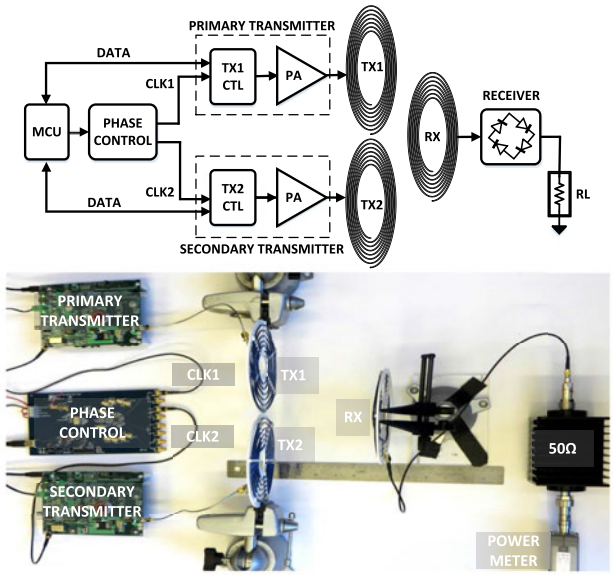

Fig. 6. System level block diagram (top), and experimental configuration using two Tx coils and one Rx coil (bottom).

$k_{\text{TX-TX}}$ range, an improvement from the two Tx and three Tx coil scenarios. Additionally, the $k_{\text{TX-TX}}$ range at which high output voltage can be achieved has also increased.

With more than one Rx coil, it is desirable to obtain adequate control of the power received at each coil. For example, while wirelessly charging multiple devices, it would be ideal to maximize efficiency to both devices simultaneously. Alternatively, if one device is finished charging and the other is still charging, power to the charged device may be nulled while power delivered to the active device may be maximized. This ability also presents a security and safety benefit in that the transmitters can control which regions receive power. For example, if a foreign object comes into contact with the transmit coil array, power in that region may be nulled while maximum power may still be delivered to actively charging devices. With one or even two Tx coils and two Rx coils, control over the regions of maximum and minimum received power is severely limited. However, additional phase-synchronized Tx coils can effectively control power delivery to two mobile Rx coils simultaneously.

Fig. 5 shows a simulated scenario where three Tx coils wirelessly power two Rx coils. The first row shows that V_o of both Rx coils can either be simultaneously powered or simultaneously nulled. When $\phi_2 = 0°$ and $\alpha_2 = 5$, V_o of both coils approaches 1 V. Similarly, by setting $\phi_2 = 170°$ and $\alpha_2 = 2$, V_o drops to nearly zero. In the first row, $\phi_3 = 0°$ while in the second row $\phi_3 = 180°$. The second row shows that V_o of one Rx coil can be maximized while V_o of the other Rx coil can be simultaneously minimized simply by tuning ϕ_2 and ϕ_3. When $\phi_2 = -110°$ and $\alpha_2 = 5$, RX_1 achieves maximum V_o while RX_2 drops to zero. Alternatively, by setting $\phi_2 = 85°$ and $\alpha_2 = 3.5$, RX_2 achieves high V_o while RX_1 drops to zero. Although this plot only indicates a snapshot of one coupling configuration between several Tx and Rx coils, these advantages can be realized for many other coil configurations at the expense of increased system complexity from the α and ϕ values associated with additional transmitters.

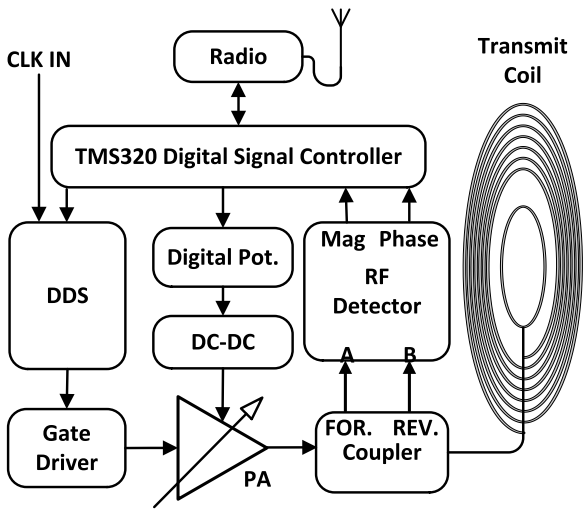

Fig. 7. Transmitter block diagram.

III. Experimental Validation of Theory

In order to validate the expressions derived in Section II, several experiments have been conducted to compare the simulated results with experimental measurements.

The hardware for the experiments is shown in Fig. 6. It comprises two independent PA that are controlled by a single MCU and a precision clock distribution circuit for phase adjustment. The clock distributor is based on the AD9510 by analog devices. Received power is measured using a 50-Ω 40-dB attenuator and Agilent U2001A RF power meter. A schematic block diagram for the transmitter board is provided in Fig. 7. The TMS320 digital signal processing unit controls all the hardware on the transmitter board including a direct digital synthesizer for frequency generation, a single-ended class E PA [20] with a programmable supply voltage determined by a digital potentiometer

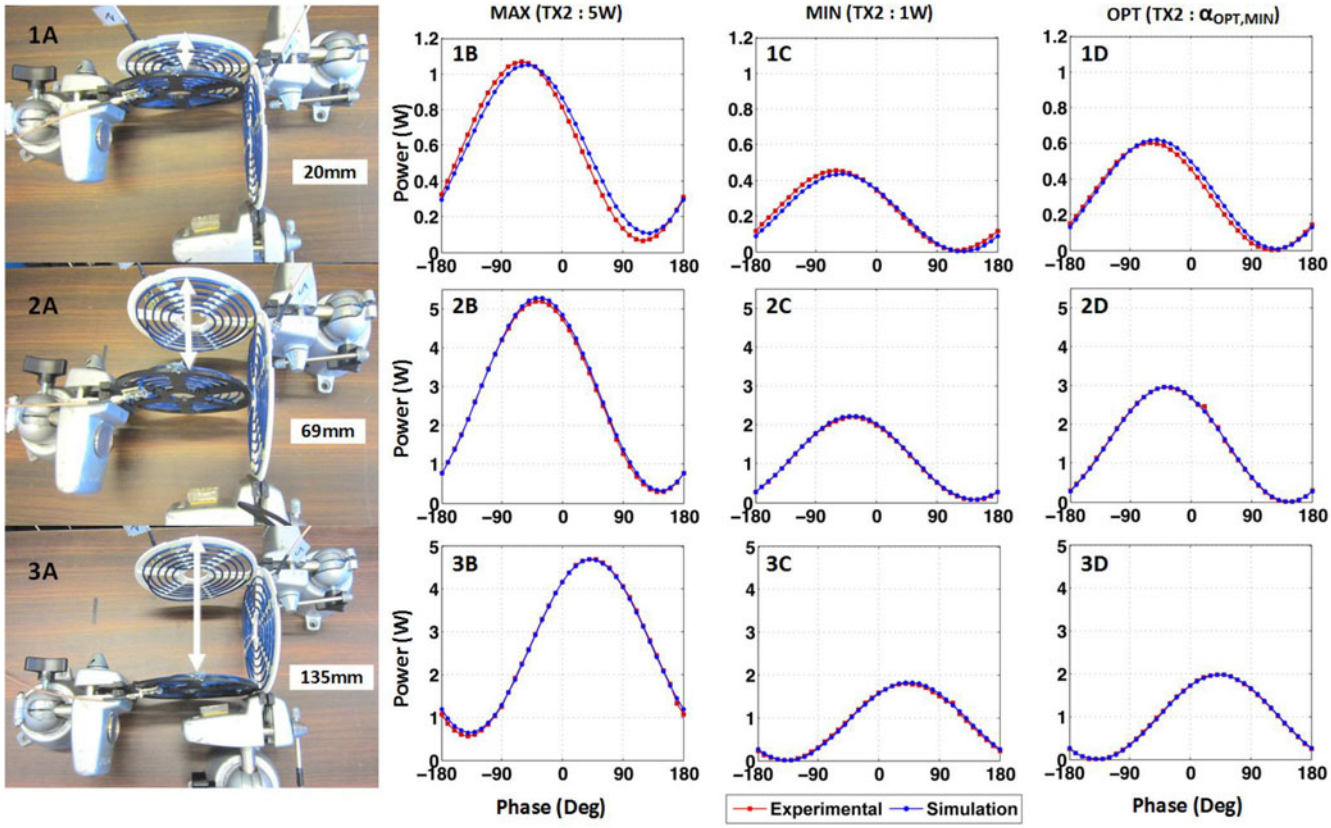

Fig. 8. Experimental and simulation results for received power corresponding to three different coil configurations and various Tx power levels.

that controls the output voltage of a dc–dc boost converter, and an RF magnitude and phase detector that analyzes the forward and reverse signals from the bidirectional coupler. The Tx and Rx coils are all identical with an inductance of $L = 17.2\ \mu$H, series tuning capacitance of $C = 8$ pF and ac resistance of $R = 1.2\ \Omega$ with a resonant frequency of 13.56 MHz.

As illustrated in Fig. 8 column A, the two Tx coils are positioned on two adjacent faces of a cube-like volume. We repositioned the Rx coil inside the volume to demonstrate different coupling configurations with each Tx coil. These positions were at 20, 69 and 135 mm from TX_1 with the Rx coil always parallel to TX_1 and orthogonal to TX_2.

At each distance, we set the output power level of TX_1 and TX_2. The output power from each transmitter was set by connecting the output of each PA directly into a 50-Ω RF power meter and adjusting the supply voltage to the PA. Relating back to the circuit analysis from Section II, the magnitude α of each sinusoidal input V_S represents the power level of each transmitter. When the transmitter with an arbitrary source resistance R_S is connected directly to a fixed load resistance R_L, V_S relates to power delivered to the load power by

$$P(W) = R_L \left(\frac{V_S}{R_S + R_L} \right)^2. \tag{9}$$

TX_1 was configured to deliver 1 W into the 50-Ω load, and remained fixed for all experiments. For the first experiment, TX_2 was configured to transmit 5 W, which corresponds to the maximum output power capability of this PA. Next, we configured TX_2 to deliver 1 W into the 50-Ω load, so that each transmitter delivers the same amount of power. Then we set the output power of TX_2 to correspond to the the value of $\alpha_{\text{opt,min}}$ for the given coupling coefficient configuration. Since $\alpha_{\text{opt,min}}$ depends on k_{12}, k_{13} and k_{23}, the power level had to change for each of the three distances in this final experiment, but was always between 1–5 W.

At each power setting and Rx coil configuration, we varied the phase of TX_2 relative to TX_1 from $-180°$ to $180°$ at $10°$ increments and recorded the received power level with the Rx coil terminated by a 50-Ω RF power meter. The experimental results are shown in Fig. 8. The red curves represent the experimental received power for each respective coil configuration.

A careful examination of these plots shows that for the same Rx coil position (i.e., same row), the minimum and maximum received power levels occur at the same ϕ value. This proves that $\phi_{\text{opt,min}}$ and $\phi_{\text{opt,max}}$ are independent of α, and only depend on the various coupling coefficients between the coils as expected from (6) and (7), respectively.

In order to validate our theoretical model, we extracted the coupling coefficients k_{12}, k_{13} and k_{23} from each of these configurations. There are direct calculations to compute coupling coefficients between two coils based on the coil geometries and distance between the coils [21]. However, for two Tx coils and one Rx coil, these approximations are not accurate. Therefore, we relied on MATLAB to identify the best-fit coupling coefficients that match the experimental results with the theoretical circuit model, given the data obtained for each of the physical

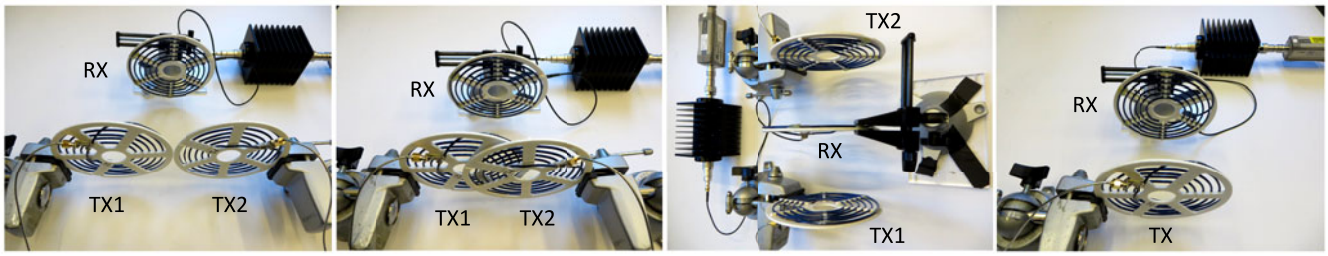

Fig. 9. Experimental coil configurations: (A) adjacent, (B) overlapping, (C) opposing, and (D) single Tx coil configurations.

configurations. Since the coupling coefficients are only dependent on coil position, the coupling coefficients are constant across different power levels. Hence, the coupling coefficients are the same for each plot in the same row in Fig. 8; however, they differ from one row to the next as the coils are repositioned.

Using these extracted coupling coefficients, along with the equivalent V_S values corresponding to the various Tx power levels (9) and the measured coil parameters ($L = 4\,\mu$H, $R = 0.95\,\Omega$ and $C = 34$ pF) of each identical Tx coil, V_o was calculated using (3) for the same range of ϕ as in the experiments. The simulated Rx power can be calculated from the output voltage measured across a 50-Ω load. These simulated results are represented by the blue curve in Fig. 8. Comparing the blue and red curves proves that our theoretical circuit model and simulation results for V_o accurately match the measured experimental results across all configurations. The maximum and minimum output power levels correspond to the calculated values of $\phi_{\mathrm{opt,max}}$ and $\phi_{\mathrm{opt,min}}$, respectively. Consider panel 1B for example: From (6) and (7), $\phi_{\mathrm{opt,min}} = 110°$, and $\phi_{\mathrm{opt,max}} = -70°$, which closely match the measured phase at which minimum and maximum power occurs for the experimental result of $104°$ and $-76°$, respectively. The expression for $\alpha_{\mathrm{opt,min}}$ can be similarly validated for any of the results from column D.

By adjusting ϕ and α at any of the three Rx positions, the received power may be minimized or maximized. As expected, the maximum output power for each configuration always occurs for maximum P_{TX2} (i.e., maximum α) in column B. Additionally, by comparing columns B and C, a much wider range of power can be delivered to the Rx coil when TX_2 outputs more power than TX_1. Although the minimum value of V_o is always greater in column B compared to column C, the difference between the peaks and troughs in column B are much wider than in column C.

The absolute minimum value of V_o always occurs when α is properly set to $\alpha_{\mathrm{opt,min}}$ in column D. This may seem counterintuitive because the power levels of TX_2 in column D are always greater than those in column C, yet column D achieves the lowest V_o. Even though V_o can be driven close to zero for each power level, the lowest V_o is always achieved in column D when the system operates at $\phi_{\mathrm{opt,min}}$ and $\alpha_{\mathrm{opt,min}}$.

IV. Additional Capabilities of Phased Array Transmitter WPT System

The phased array WPT system has several advantages over a single Tx coil configuration. However, the configuration of the transmit coils and the magnitude and phase of each transmitter all must be set properly to realize the advantages. In this section, we identify the ideal operating conditions and the optimal Tx coil configuration of a phased array WPT system. We also demonstrate some additional capabilities of the system including reduced leakage field strength, and an automatic tuning algorithm that dynamically controls the magnitude and phase for minimum or maximum power transferred to the Rx coil.

Four different physical coil configurations have been evaluated as shown in Fig. 9. The first three all use two phase-synchronized Tx coils, and the last uses a single Tx coil. In the adjacent configuration [see Fig. 9(A)], the two Tx coils are side by side to one another, where they are strongly coupled. In the overlapping configuration [see Fig. 9(B)], the two Tx coils are positioned so that the magnetic fields generated by each coil destructively interfere creating a null in flux linkage between the two Tx coils. Therefore, the coupling between the Tx coils in the overlapping configuration is very close to zero. In the opposing configuration [see Fig. 9(C)], the two Tx coils are on opposite sides of the Rx coil. The coupling between the two Tx coils is very small in this configuration, and the Rx coil acts like a relay resonator between the two Tx coils. This configuration could be very practical in a hallway, where Tx coils are lined up on both sides of the hallway. Finally, the single Tx coil configuration [see Fig. 9(D)] shows the experimental setup for the nonphased array WPT system.

A. Experimental Comparison of Tx Coil Configurations

To compare the various Tx coil configurations, each Tx coil was driven by a class-E PA operating at 13.56 MHz and a fixed output power of 1.5 W when terminated in a 50-Ω load. However, it should be noted that the power from the PA to the Tx coil will change as the load impedance presented to the PA changes. In other words, even though the supply voltage to the class-E PA is fixed at 10 V for all these experiments, the amount of power consumed by the PA and the RF output power from the PA will change as the distance between the Tx and Rx coils changes and as the phase between the two Tx coils changes. The Rx coil was terminated in a 50-Ω 40-dB attenuator and RF power meter. We manually varied the phase difference between the two Tx coils from $-180°$ to $180°$ in increments of $10°$. This procedure was repeated for three different separation distances between the Tx coil(s) and the Rx coil of 4, 8 and 12 cm.

At each phase setting and for every distance, we measured the dc power supplied to each transmitter P and the RF

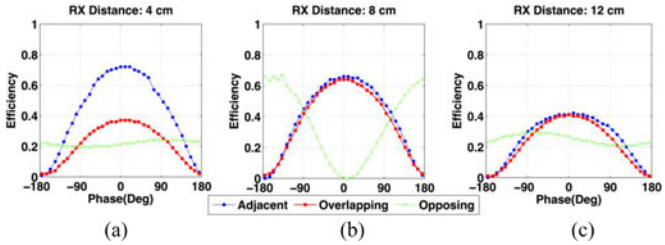

Fig. 10. System dc-RF efficiency for three different Tx coil configurations.

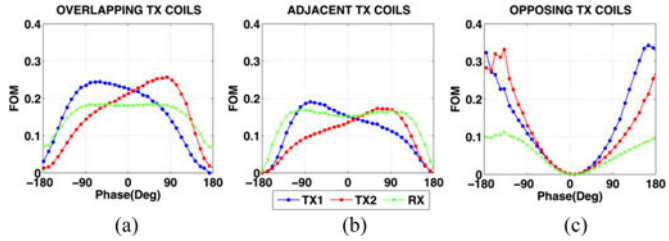

Fig. 11. FOM measured at three separate locations: behind TX_1, behind TX_2 and behind the RX coil for an 8 cm separation between the Tx coils and the Rx coil.

receive power at the output of the Rx coil $P_{\text{RF,RX}}$. The total input power P_{IN} can be calculated by adding the dc power supplied to each transmitter. The system dc-RF efficiency $\eta_{\text{DC-RF}}$ is calculated using (10)

$$\eta_{\text{DC-RF}} = \frac{P_{\text{OUT}}}{P_{\text{IN}}} = \frac{P_{\text{RF,RX}}}{P_{\text{IN,TX1}} + P_{\text{IN,TX2}}}. \tag{10}$$

Fig. 10(A)–(C) shows the efficiency plotted against phase. The adjacent configuration provides the highest achievable efficiency at each distance. At the closest distance of 4 cm, the adjacent configuration is the only one that can overcome the frequency splitting effect caused by the strong coupling between the Tx and Rx coils [22]. At distances of 8 and 12 cm, the overlapping configuration performs almost as well as the adjacent configuration, but is always slightly below the efficiency achieved by the adjacent configuration. At first this seems counter-intuitive because it would seem that when the coupling between the Tx coils is stronger as in the adjacent configuration, more energy would be coupled between the Tx coils and thus more energy would be dissipated across the ac resistance of the Tx coils. This would be true if the PA efficiency is neglected and only the coil-coil efficiency was measured. Since the amplifier efficiency is also included and given that the amplifiers are optimized to drive a 50-Ω load, the amplifiers are most efficient in the adjacent configuration because the critically-coupled Tx coils present close to a 50-Ω load, regardless of the distance between the Tx and Rx coils. Finally, the opposing configuration only matches the peak efficiency of the adjacent and overlapping configurations at the distance of 8 cm, which happens to be when the Rx coil is perfectly centered between the two Tx coils. However, the peak efficiency at 8 cm occurs for a phase of 180°. At 4 and 12 cm, the Rx coil is strongly coupled to one of the Tx coils, therefore the opposing transmitter would need to significantly increase its magnitude in order to have a more noticeable impact on efficiency.

During the same experiment, the magnetic field (H-field) strength was measured at three separate locations using the ETS-Lindgren Holaday HI-2200 H-field probe. The locations include behind TX_1, behind TX_2, and behind the Rx coil. Minimizing the magnetic field strength, or leakage fields around the Tx and Rx coils is important for practical applications for both regulatory compliance with human safety and minimal interference with surrounding objects, particularly sensitive electronics [7], [23].

Since the amount of transmit and receive power varies as the phase difference between TX_1 and TX_2 changes, it would be an unfair comparison to only account for the measured magnetic field strength. Therefore, a figure of merit (FOM) has been defined in (11) to determine the coil configuration that achieves both high efficiency and low leakage fields. The units of this FOM are inverse of the H-field, or $(\frac{A}{m})^{-1}$

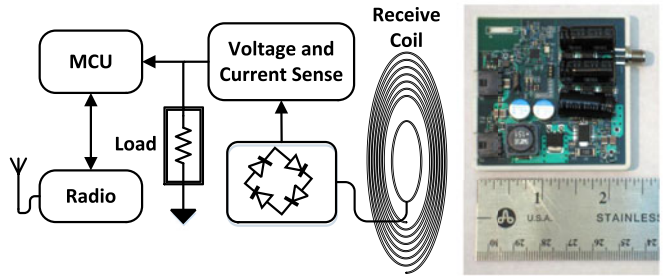

Fig. 12. Receiver block diagram (left) and photo of receiver circuit (right).

$$\text{FOM} = \frac{\eta}{H} = \frac{P_{\text{OUT}}}{P_{\text{IN}}} \times \frac{1}{H}. \tag{11}$$

To compare the field strength FOMs at the Tx and Rx coils, Fig. 11 shows the FOM at each H-field probe location (TX_1, TX_2, and Rx coils) for each configuration at an 8-cm separation distance. The configuration with the highest FOM implies that it has high efficiency and low leakage fields. With weak coupling between the Tx coils, the overlapping configuration has the highest overall FOM across all H-field measurement positions. With strong coupling between the Tx coils, the adjacent configuration achieves a lower FOM than the overlapping configuration behind the Tx coils, but it achieves a similar FOM behind the Rx coil. The opposing configuration has the highest peak FOM behind the Tx coils. However, the Rx coil is surrounded on both sides by TX_1 and TX_2 in this configuration, and consequently the FOM at the Rx coil is the lowest across all configurations.

B. Automatic Tuning

Prior work has used adaptive frequency tracking and adaptive impedance matching to automatically tune WPT systems for maximum efficiency [22], [24]–[26]. In this section, automatic tuning will be implemented by dynamically controlling the magnitude and phase of each transmitter. All of the experiments up to this point have used a 50-Ω load terminating the Rx coil. Now, this 50-Ω load will be replaced with a custom-built PCB shown in Fig. 12. The receiver consists of a full-bridge

rectifier, voltage and current sense amplifier circuitry to accurately measure the dc voltage and current at the output of the rectifier, and an MSP430 micro controller unit and CC2500 2.4-GHz radio to communicate the received power data back to the wireless power transmitter circuit.

The output voltage delivered to the load is the unregulated rectified voltage. However, the rectified voltage can be maintained at a fixed voltage with a tolerance of 0.1% by the out-of-band feedback loop alone. For this experiment, 12 V was selected arbitrarily as the regulated output voltage, but any other voltage can be defined in software as the target rectified voltage. If the measured voltage is above or below $12\ V \pm 1\%$, then the transmitter automatically decreases or increases the transmit power level, respectively. The advantage of this power-tracking feedback loop is that the power delivered to the load can be fixed without any additional dc–dc converters, which can be costly and consume precious PCB area.

For a two-Tx and one-Rx phased array WPT system, an automatic-tuning (autotuning) algorithm has been developed that dynamically controls both the amplitude and phase of TX_2 relative to TX_1. From (7), the optimal phase $\phi_{\mathrm{opt,max}}$ is independent of α. Therefore, the phase that achieves the highest measured rectified voltage is $\phi_{\mathrm{opt,max}}$. Ideally, this value could be computed directly from (7), but in this implementation we perform an exhaustive phase sweep and hone in on the phase that results in the highest rectified voltage. Once $\phi_{\mathrm{opt,max}}$ has been set, power-tracking takes over and identifies the minimum transmit power level to maintain the 12-V rectified voltage on the receiver. At this point, system efficiency has been automatically optimized, and the algorithm will repeat once the coils move, which can be detected by a change in the rectified voltage

$$\eta_{\text{DC-DC}} = \frac{P_{\text{OUT}}}{P_{\text{IN}}} = \frac{V_{\text{RECT}} \times I_{\text{RECT}}}{P_{\text{IN,TX1}} + P_{\text{IN,TX2}}}. \tag{12}$$

Autotuning has been applied to the experimental setup to compare the system dc–dc efficiency (12) of a phased array system to a single Tx coil system. The experimental setup is identical to Fig. 6 except the 50-Ω attenuator has been replaced by the receiver circuit. The HP 6063B dc electronic load acted as a constant power load, set to sink a constant current of 100 mA at a rectified voltage of 12 V, therefore dissipating 1.2 W. We arranged the Tx coils in the adjacent configuration. It is important to note that although the adjacent configuration achieves a lower FOM compared to the overlapping Tx coil configuration, we selected the adjacent configuration for this experiment because it resulted in the highest overall efficiency from Fig. 10.

TX_1 was set to a fixed transmit power level, while TX_2 was placed in autotuning mode. We changed the distance between the Tx and Rx coils from 1–16 cm at 1 cm increments and measured $\eta_{\text{DC-DC}}$ at each distance after the autotuning algorithm stabilized. Fig. 13 shows the efficiency as a function of distance between the coils.

The various curves on Fig. 13 correspond to different Rx coil positions relative to the Tx coils. The black curve on Fig. 13 shows the result when the Rx coil was placed at the center of the two Tx coils, identical to the configuration shown in Fig. 9(A). The green curve corresponds to the configuration when the Rx coil was placed directly in front of TX_2, respectively. Finally, the red curve represents the single Tx coil case when TX_1 was removed altogether and the Rx coil was placed directly in front TX_2.

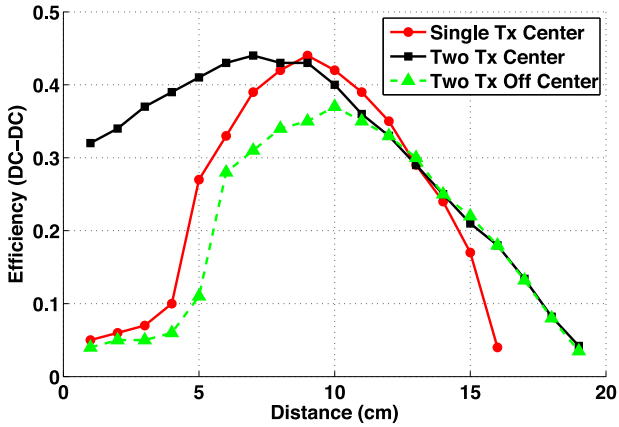

Fig. 13. Efficiency versus distance comparisons with autotuning enabled.

Highest efficiency can be achieved when the Rx coil is placed directly between the two Tx coils. Compared to the single Tx configuration, the phased array configuration achieves higher efficiency when the coils are close together. The phased array WPT system can overcome the frequency splitting effect caused by strong coupling between the Tx and Rx coils, which causes poor efficiency for the single Tx coil configuration at distances less than 9 cm. At approximately 10 cm, which corresponds to the critically coupled position, the single Tx configuration achieves a higher peak efficiency than the centered Rx coil phased array system. However, as the distance continues to increase, the phased array system efficiency declines slower and maintains higher efficiency beyond 15 cm.

When the Rx coil is placed directly in front of TX_2 in the phased array configuration, the efficiency is almost always worse than the single coil configuration. This occurs because, although one transmitter is very strongly coupled to the Rx coil, the adjacent transmitter is very weakly coupled to the Rx coil, and ultimately degrades system efficiency since it contributes very little to the received power while transmitting a substantial amount of power. In this scenario, system efficiency could be improved by disabling TX_1 altogether. However, when the Rx coil exceeds 15 cm, the phased array system achieves higher efficiency.

In summary, the phased array WPT system can achieve higher system efficiency when the Rx coil is close and centrally located between the two Tx coils or when the Rx coil is sufficiently far from the Tx coils. However, when the Rx coil is in between these two regions, higher system efficiency can be achieved by disabling the transmitter that is located farthest away from the Rx coil.

V. Conclusion

In this paper, we argue that phased array WPT systems can have advantages in terms of system efficiency and minimal leakage fields if the phased array system is designed and implemented properly. Proper design and implementation requires a

rigorous understanding of the circuits and controllable parameters for a phased array WPT system. We provide a thorough analysis of a generalized multiple transmitter, multiple receiver phase-synchronized WPT system that can be used to quickly simulate complex networks of wireless power transmitters and receivers. We expand on this analysis and demonstrate simulation results for three and four Tx coil phased array WPT systems.

The remainder of the paper focuses on a three-element system, consisting of two Tx coils and one Rx coil. We define critical parameters that allow the user to directly compute the magnitude and phase that either maximizes or minimizes power delivered to the load. After experimentally validating these equations and simulation results, we highlight some additional capabilities of a phased array WPT system in comparison to a standard single Tx coil configuration. The adjacent phased array configuration achieves highest system efficiency, which includes the PA efficiency on the transmitter side and rectifier efficiency on the receive side. However, the overlapping configuration results in lowest leakage fields behind the Tx coils, and consequently the highest FOM for the best balance between high efficiency and low leakage fields. Finally, we present a fully autonomous system capable of adapting to variations in distance between the Tx and Rx coils while automatically controlling the magnitude and phase of the transmitter to maintain maximum system efficiency.

ACKNOWLEDGMENT

The authors would like to thank members of the Sensor Systems Research Group for their thoughts and contributions to this study.

REFERENCES

[1] B. Waters, B. Mahoney, G. Lee, and J. Smith, "Optimal coil size ratios for wireless power transfer applications," in *Proc. IEEE Int. Symp. Circuits Syst.*, Jun. 2014, pp. 2045–2048.

[2] R. Johari, J. Krogmeier, and D. Love, "Analysis and practical considerations in implementing multiple transmitters for wireless power transfer via coupled magnetic resonance," *IEEE Trans. Ind. Electron.*, vol. 61, no. 4, pp. 1774–1783, Apr. 2014.

[3] J. Casanova, Z. N. Low, and J. Lin, "A loosely coupled planar wireless power system for multiple receivers," *IEEE Trans. Ind. Electron.*, vol. 56, no. 8, pp. 3060–3068, Aug. 2009.

[4] A. Uchida, S. Shimokawa, H. Kawano, K. Ozaki, K. Matsui, and M. Taguchi, "Phase and intensity control of multiple coil currents in mid-range wireless power transfer," *IET Microwaves, Antennas Propag.*, vol. 8, no. 7, pp. 498–505, May 2014.

[5] J. Jadidian and D. Katabi, "Magnetic mimo: How to charge your phone in your pocket," in *Proc. 20th Annu. Int. Conf. Mobile Comput. Netw.*, 2014, pp. 495–506.

[6] D. Ahn and S. Hong, "Effect of coupling between multiple transmitters or multiple receivers on wireless power transfer," *IEEE Trans. Ind. Electron.*, vol. 60, no. 7, pp. 2602–2613, Jul. 2013.

[7] *Electronic Code of Federal Regulations*, *Part 15: Radio Frequency Devices*, F. C. Commission, vol. Title 47: Telecommunication (47CFR15), 2014.

[8] N. Oodachi, K. Ogawa, H. Kudo, H. Shoki, S. Obayashi, and T. Morooka, "Efficiency improvement of wireless power transfer via magnetic resonance using transmission coil array," in *Proc. IEEE Int. Symp. Antennas Propag.*, Jul. 2011, pp. 1707–1710.

[9] O. Jonah, S. Georgakopoulos, and M. Tentzeris, "Orientation insensitive power transfer by magnetic resonance for mobile devices," in *Proc. IEEE Wireless Power Transfer*, May 2013, pp. 5–8.

[10] J. Hsu, A. Hu, P. Si, and A. Swain, "Power flow control of a 3-d wireless power pick-up," in *Proc. 2nd IEEE Conf. Ind. Electron. Appl.,* May 2007, pp. 2172–2177.

[11] P. Raval, D. Kacprzak, and A. Hu, "A wireless power transfer system for low power electronics charging applications," in *Proc. 6th IEEE Conf. Ind. Electron. Appl.*, Jun. 2011, pp. 520–525.

[12] W. M. Ng, C. Zhang, D. Lin, and S. Hui, "Two- and three-dimensional omnidirectional wireless power transfer," *IEEE Trans. Power Electron.*, vol. 29, no. 9, pp. 4470–4474, Sep. 2014.

[13] A. P. Sample, D. A. Meyer, and J. R. Smith, "Analysis, experimental results, and range adaptation of magnetically coupled resonators for wireless power transfer," *IEEE Trans. Ind. Electron.*, vol. 58, no. 2, pp. 544–554, Feb. 2011.

[14] A. E. Fouda, F. L. Teixeira, and M. E. Yavuz, "Time-reversal techniques for miso and mimo wireless communication systems," *Radio Sci.*, vol. 47, no. 6, pp. 1–15, 2012.

[15] A. Massa, G. Oliveri, F. Viani, and P. Rocca, "Array designs for long-distance wireless power transmission: State-of-the-art and innovative solutions," *Proc. IEEE*, vol. 101, no. 6, pp. 1464–1481, Jun. 2013.

[16] D. Arnitz and M. Reynolds, "Wireless power transfer optimization for nonlinear passive backscatter devices," in *Proc. IEEE Int. Conf. RFID*, Apr. 2013, pp. 245–252.

[17] I. Gupta and A. Ksienski, "Effect of mutual coupling on the performance of adaptive arrays," *IEEE Trans. Antennas Propag.*, vol. 31, no. 5, pp. 785–791, Sep. 1983.

[18] R. Islam and R. Adve, "Beam-forming by mutual coupling effects of parasitic elements in antenna arrays," in *Proc. IEEE Antennas Propag. Soc. Int. Symp.*, 2002, pp. 126–129.

[19] S. Raju, R. Wu, M. Chan, and C. Yue, "Modeling of mutual coupling between planar inductors in wireless power applications," *IEEE Trans. Power Electron.*, vol. 29, no. 1, pp. 481–490, Jan. 2014.

[20] Z. N. Low, R. Chinga, R. Tseng, and J. Lin, "Design and test of a high-power high-efficiency loosely coupled planar wireless power transfer system," *IEEE Trans. Ind. Electron.*, vol. 56, no. 5, pp. 1801–1812, May 2009.

[21] C. Zierhofer and E. Hochmair, "Geometric approach for coupling enhancement of magnetically coupled coils," *IEEE Trans. Biomed. Eng.*, vol. 43, no. 7, pp. 708–714, Jul. 1996.

[22] A. Sample, B. Waters, S. Wisdom, and J. Smith, "Enabling seamless wireless power delivery in dynamic environments," *Proc. IEEE*, vol. 101, no. 6, pp. 1343–1358, Jun. 2013.

[23] A. Christ, M. Douglas, J. Roman, E. Cooper, A. Sample, B. Waters, J. Smith, and N. Kuster, "Evaluation of wireless resonant power transfer systems with human electromagnetic exposure limits," *IEEE Trans. Electromagn. Compat.*, vol. 55, no. 2, pp. 265–274, Apr. 2013.

[24] B. H. Waters, A. P. Sample, and J. R. Smith, "Adaptive impedance matching for magnetically coupled resonators," in *Proc. Progress Electromagn. Res. Symp.*, Aug. 2012, pp. 694–701.

[25] Y. Lim, H. Tang, S. Lim, and J. Park, "An adaptive impedance-matching network based on a novel capacitor matrix for wireless power transfer," *IEEE Trans. Power Electron.*, vol. 29, no. 8, pp. 4403–4413, Aug. 2014.

[26] S. Aldhaher, P.-K. Luk, and J. Whidborne, "Electronic tuning of misaligned coils in wireless power transfer systems," *IEEE Trans. Power Electron.*, vol. 29, no. 11, pp. 5975–5982, Nov. 2014.

Benjamin H. Waters (S'10) received the B.A. degree in physics from Occidental College, Los Angeles, CA, USA, in 2010, and the B.S. degree in electrical engineering from Columbia University, New York, NY, USA, in 2010, and the M.S. degree in electrical engineering from the University of Washington, Seattle, WA, USA, in 2012. He is currently working toward the Ph.D. degree in electrical engineering at the University of Washington.

As an undergraduate, he worked in the Columbia Integrated Systems Laboratory, Columbia University, where he completed research on wireless power transfer. He has several internship experiences with Network Appliance, Arup, Intel Labs Seattle, and most recently with Bosch in 2013 where he continued his research in wireless power transfer. His research interests lie mostly in the field of wireless power, including near-field antenna design, adaptive maximum power point tracking systems, and applications for these systems including biomedical, military, and consumer electronics.

Mr. Waters is a Member of Tau Beta Pi and Pi Mu Epsilon.

Brody J. Mahoney (M'09) received the B.S. degree in electrical and electronic engineering from California State University, Sacramento, CA, USA, in 2009. He is currently a Graduate Student at the University of Washington, Seattle, WA, USA, where he is working toward the Ph.D. degree in electrical engineering.

After receiving his B.S. degree, he worked for more than three years with naval-reactor control systems at Puget Sound Naval Shipyard, Bremerton, WA, USA. In 2012, he joined the Sensor Systems Research Group, University of Washington. His research interests comprise wireless power and adaptive low-power mixed-mode VLSI systems for sensing applications.

Mr. Mahoney is a Member of Tau Beta Pi and Phi Kappa Phi.

Vaishnavi Ranganathan (M'13) received the B.Tech. degree in electronics and instrumentation engineering from Amrita Vishwavidyapeetham University, Coimbatore, India, in 2011, and the M.S. degree in electrical engineering, specializing in NEMS, from Case Western Reserve University, Cleveland, OH, USA, in 2013. She is currently working toward the Ph.D. degree at the Sensor Systems Laboratory, University of Washington, Seattle, WA, USA.

Her main research interests are wireless power and brain–computer interface applications, including low-power computation and communication solutions for implantable devices. As an undergraduate, she gained experience in robotics and was a Member of SAE-India.

Joshua R. Smith (M'99) received the B.A. degree in computer science and philosophy from Williams College, Williamstown, MA, USA, the M.A. degree in physics from Cambridge University, Cambridge, U.K., and the Ph.D. and S.M. degrees from the MIT Media Lab, Cambridge, MA, USA.

He is an Associate Professor of electrical engineering and of computer science and engineering at the University of Washington, Seattle, WA, USA, where he leads the Sensor Systems Research Group. From 2004 to 2010, he was Principal Engineer at Intel Labs Seattle. He is interested in all aspects of sensor systems, including creating novel sensor systems, powering them wirelessly, and using them in applications such as robotics, ubiquitous computing, and human computer interaction. At Intel, he founded and led the Wireless Resonant Energy Link Project, as well as the Wireless Identification and Sensing Platform Project, and the Personal Robotics Project. Previously, he coinvented an electric field sensing system for suppressing unsafe airbag firing that is included in every Honda car.